bioRxiv preprint doi: https://doi.org/10.1101/2020.09.12.294801; this version posted September 13, 2020. The copyright holder for this preprint (which was not certified by peer review) is the author/funder. All rights reserved. No reuse allowed without permission.

Quantifying cytoskeletal heterogeneity via single-cell protein-complex fractionation

Julea Vlassakis, Ph.D.[1,†], Louise L. Hansen[1,†], Ryo Higuchi-Sanabria, Ph.D.[2], Yun Zhou[3], C. Kimberly Tsui, Ph.D.[2], Andrew Dillin, Ph.D.[2,4], Haiyan Huang, Ph.D.[5,6] and Amy E. Herr, Ph.D.[1,*]

1. Department of Bioengineering, University of California Berkeley, Berkeley, California 94720, United States.
2. Department of Molecular and Cell Biology, University of California Berkeley, Berkeley, California 94720, United States.
3. Division of Biostatistics, University of California Berkeley, Berkeley, California 94720, United States.
4. Howard Hughes Medical Institute, University of California Berkeley, Berkeley, California 94720, United States.
5. Department of Statistics, University of California Berkeley, Berkeley, California 94720, United States.
6. Center for Computational Biology, University of California Berkeley, Berkeley, California 94720, United States.

[†] These authors contributed equally.
*Corresponding Author: Amy E. Herr, aeh@berkeley.edu

bioRxiv preprint doi: https://doi.org/10.1101/2020.09.12.294801; this version posted September 13, 2020. The copyright holder for this preprint (which was not certified by peer review) is the author/funder. All rights reserved. No reuse allowed without permission.

Abstract

Multimeric cytoskeletal protein complexes, including filamentous F-actin, orchestrate normal cellular function. However, protein-complex distributions in stressed, heterogeneous cell populations remain unknown. Cell staining and proximity-based methods have limited selectivity and/or sensitivity for robust endogenous multimeric protein-complex quantification from single cells. We introduce micro-arrayed differential detergent fractionation to simultaneously detect protein complexes in 100s of individual cells. Fractionation occurs by 60s size-exclusion electrophoresis with protein complex-stabilizing buffer that minimizes depolymerization. Validating with actin-destabilizing Latrunculin A (LatA), we quantify 2.7-fold lower median F-actin complex-levels in LatA-treated single cells. Further clustering analysis of U2OS cells treated with LatA detects a subpopulation (~11%) exhibiting downregulated F-actin, but upregulated microtubule and intermediate filament protein complexes. Thus, some cells upregulate other cytoskeletal complexes to counteract the stress of LatA treatment. We also sought to understand the effect of non-chemical stress on cellular heterogeneity of F-actin, and find heat shock dysregulates F and monomeric G-actin correlation. The assay overcomes selectivity limitations of existing methods to biochemically quantify single-cell protein complexes perturbed with diverse stimuli.

Introduction

Over 80,000 protein complexes comprised of interacting proteins regulate processes from proteostasis to transcription[1]. A critical set of protein complexes form the cell cytoskeleton. The cytoskeletal protein actin dynamically polymerizes and depolymerizes[2,3] between monomeric G-actin (~42 kDa) and filamentous F-actin[4] states to determine cell morphology, motility, and proliferation[5]. F-actin is considered the "functional" actin species in the cytoskeleton. Thus, the F-actin ratio (or F-actin divided by total actin) is a metric for cytoskeletal integrity. F-actin levels can be increased in metastatic cancer cells,[5] thus underpinning the design of oncology drugs that disrupt F-actin filaments[6]. Quantifying the distribution of cytoskeletal protein complexes in single cells would inform drug development and elucidate stress-induced cancer transformations.

To understand cytoskeletal protein-complex expression heterogeneity, no method combines the needed detection sensitivity, throughput, and selectivity for multimeric protein complexes in single cells. Top-down mass spectrometry determines protein-complex stoichiometry after lossy sample fractionation that prevents low cell number protein-complex identification[7] (unlike single-cell bottom-up mass spectrometry[8,9]). Targeted approaches such as proximity ligation assay and FRET achieve single-cell sensitivity, but rely on adjacent oligo-bound antibodies or fluorescent probes to infer two proteins are interacting[10,11]. Multi-component or multimeric protein complexes are difficult to detect with such proximity-based techniques. Finally, actin-specific detection methods suffer from limitations impacting sensitivity and selectivity. Visualization of the actin cytoskeleton relies on fluorescently tagged actin (e.g., GFP-actin fusion or split GFP-actin fusion[12]), GFP-fused actin binding proteins or peptides (e.g., Lifeact, F-tractin, Utrophin), nanobodies[13], or chemicals that directly bind actin (e.g., phalloidin). Such molecules may alter cytoskeletal dynamics both *in vitro* and *in vivo*[14–16]. Phalloidin competes with endogenous actin-binding proteins[17] and actin-targeting drugs, such as Jasplakinolide[18]. Bulk ultracentrifugation is another approach, wherein mild lysis in F-actin stabilization buffer solubilizes G-actin and preserves F-actin. The supernatant (G-actin) and pellet (F-actin) fractions are subsequently

bioRxiv preprint doi: https://doi.org/10.1101/2020.09.12.294801; this version posted September 13, 2020. The copyright holder for this preprint (which was not certified by peer review) is the author/funder. All rights reserved. No reuse allowed without permission.

quantified by western blotting or DNase inhibition assay[19]. However, bulk ultracentrifugation typically requires ~10^7 cells, masking underlying cell-to-cell variation[19].

To address gaps in multimeric protein-complex quantification, we introduce "Single-cell protein Interaction Fractionation Through Electrophoresis and immunoassay Readout", or SIFTER. We separate protein complexes from monomers with differential detergent fractionation and electrophoresis in the SIFTER gel stippled with microwells for in-situ single-cell lysis. The gel size-excludes protein complexes larger than ~740 kDa, while the <1 mm height of the conductive SIFTER device minimizes resistive heating that would prematurely depolymerize F-actin complexes. With efficient heat dissipation, we fractionate protein complexes in less than one minute, or 40x faster than ultracentrifugation. Hundreds of multi-stage, 1-mm fractionation separations are performed simultaneously in the open gel array (microscope slide-sized). Both the protein complex (e.g., F-actin) and monomer (e.g., G-actin) states are blotted or immobilized in distinct regions abutting each microwell. Protein complex and monomer states are quantified by in-gel immunoprobing, allowing detection of multiple protein targets[20]. We applied SIFTER to four basic questions. First, we asked what is the distribution of the F-actin ratio across a population of single cells? Second, we sought to understand whether two well-studied actin-targeting drugs (Latrunculin A and Jasplakinolide) induced variation in F-actin complex-levels in single cells compared to controls. Third, as a corollary, we inquired whether Latrunculin A yields cellular phenotypes distinct from controls with differential expression of other cytoskeletal protein complexes such as microtubules and intermediate filaments. Fourth, we asked how heat shock, another cellular stress, shifts the F-actin ratio distribution and coordination between F- and G-actin at the single-cell level. We show SIFTER is a versatile method for understanding cellular heterogeneity – at single-cell resolution – in protein-complex levels in response to perturbation.

Results

SIFTER design principles and characterization

To selectively detect cytoskeletal protein complexes from single cells, we integrate differential detergent fractionation, electrophoretic separation, and immunoassay steps into a single microdevice. An important dynamic protein complex is the F-actin filament. Each filament can be composed of up to 100s of globular G-actin monomers (k_{off} ~ 0.2 - 1.0 s^{-1} *in vivo*[21]; Fig. 1a). Two design considerations are central to our actin measurement: (1) discerning actin state (F- vs. G-actin); and (2) maintaining F-actin complexes during fractionation. For the first design consideration, F-actin polymerization proceeds rapidly once four G-actin are incorporated in a filament. Steady-state polymerization (k_{on} ~0.1-5 $\mu M^{-1}s^{-1}$)[21] yields a distribution of filament masses, averaging ~2700 kDa[22]. While the F-actin mass distribution below ~2700 kDa is unknown *in vivo*, F-actin is highly enmeshed. Thus, discerning F- (<160 kDa) vs. G-actin (42 kDa) requires coarse size cutoff (~100s of kDa). On the second design consideration, rapid F-actin depolymerization occurs below the critical concentration of total actin (~0.2 - 2.0 μM *in vivo*). To maintain local concentrations of actin above the critical concentration requires no greater than ~10-fold dilution during the assay, as cellular total actin is ~10-100 μM. Thus, the SIFTER fractionation gel contains microwells with ~10^8-fold smaller reaction volume versus bulk ultracentrifugation to minimize dilution. The microwells accommodate gravity-sedimented single cells[20] within the open, fractionation gel (Fig. 1a). The open device is suited to rapid serial introduction of buffers via a hydrogel lid to first

bioRxiv preprint doi: https://doi.org/10.1101/2020.09.12.294801; this version posted September 13, 2020. The copyright holder for this preprint (which was not certified by peer review) is the author/funder. All rights reserved. No reuse allowed without permission.

lyse cells and stabilize F-actin during fractionation, and then depolymerize F-actin to spatially separate the F- vs. G-actin states (Fig. 1b-c).

To report both the state and relative amount of actin per cell, SIFTER comprises five assay steps (Fig. 1c). First, single cells settled in microwells are lysed in an F-actin stabilization buffer delivered by the hydrogel lid, creating a lysate containing the two actin states. Second, F-actin complexes are fractionated from the smaller G-actin monomers by polyacrylamide gel electrophoresis (EP, 60 s), during which the larger F-actin is size-excluded from the gel and retained in each microwell. Once G-actin monomers electrophorese into the gel, these actin monomers are immobilized (blotted) using a UV-induced covalent reaction to benzophenone methacrylamide integrated into the gel polymer network[20]. Third, to depolymerize the F-actin complexes retained in each microwell, a protein-complex depolymerization buffer is introduced by another hydrogel lid. Fourth, we electrophorese the now depolymerized F-actin complexes into a region of the gel separate from the immobilized monomers, where they are in turn immobilized. Fifth, in-gel immunoprobing detects the immobilized populations of G-actin monomer and monomer depolymerized from the F-actin complexes (Fig. 1e) using a fluorescently labeled antibody against G-actin.

To maintain intact F-actin complexes in each microwell during G-actin EP fractionation, the F-actin stabilization buffer slows the natural depolymerization kinetics. The non-ionic detergent Triton X-100[19,23] at ~1% v/v lyses the cell and minimally alters in vitro polymerization rates of actin[24]. Addition of 2 mM $MgCl_2$ stabilizes F-actin complexes[19], as Mg^{2+} binds each G-actin to lower depolymerization rates[22]. Consequently, only ~2% of total F-actin depolymerizes per minute in mammalian cells lysed in stabilization buffer[19], motivating our goal to fractionate in ~1 minute. Cell lysis depends on Triton-X 100 micelle diffusion to the bottom of the microwells, which requires only ~10s[25]. Imaging release of monomeric G-actin fused to fluorescent GFP from GFP-actin expressing breast cancer cells (MDA-MB-231 GFP-actin) confirms a 45s lysis yields only ~2.5-4x dilution of total actin to remain above the critical concentration (Fig. 1d).

Validation and benchmarking SIFTER

We first validated SIFTER by fractionating and quantifying the G-actin monomer vs. F-actin complexes in each of the MDA-MB-231 GFP-actin cells. We selected GFP-actin expressing cells so that we could utilize fluorescence imaging to optimize cell lysis (Fig. 1d) and EP conditions. Immunoprobing for GFP yields distinct Gaussian protein peaks corresponding to GFP G-actin (G) on the right and GFP F-actin (F) to the left of each microwell (Fig. 1e). By summing the area-under-the-curve of G and F, we calculate the *F-actin ratio* (F_{ratio}) = $F / (F+G)$ for each cell. The MDA-MB-231 GFP-actin fusion cell average $F_{ratio} = 0.44 \pm 0.11$ (standard deviation; n = 331 cells, from N = 3 SIFTER devices measured on the same day), in reasonable agreement *with* F_{ratio} ~0.5 for MDA-MB-231 from bulk ultracentrifugation[26]. With SIFTER, the F_{ratio} coefficient of variation is 25%, revealing single-cell variation obscured in the bulk assay. Important to minimizing F-actin-complex depolymerization during the assay, SIFTER completes cell lysis and fractionation in <5 minutes, or ~40 times faster than bulk ultracentrifugation (Fig. 1f).

bioRxiv preprint doi: https://doi.org/10.1101/2020.09.12.294801; this version posted September 13, 2020. The copyright holder for this preprint (which was not certified by peer review) is the author/funder. All rights reserved. No reuse allowed without permission.

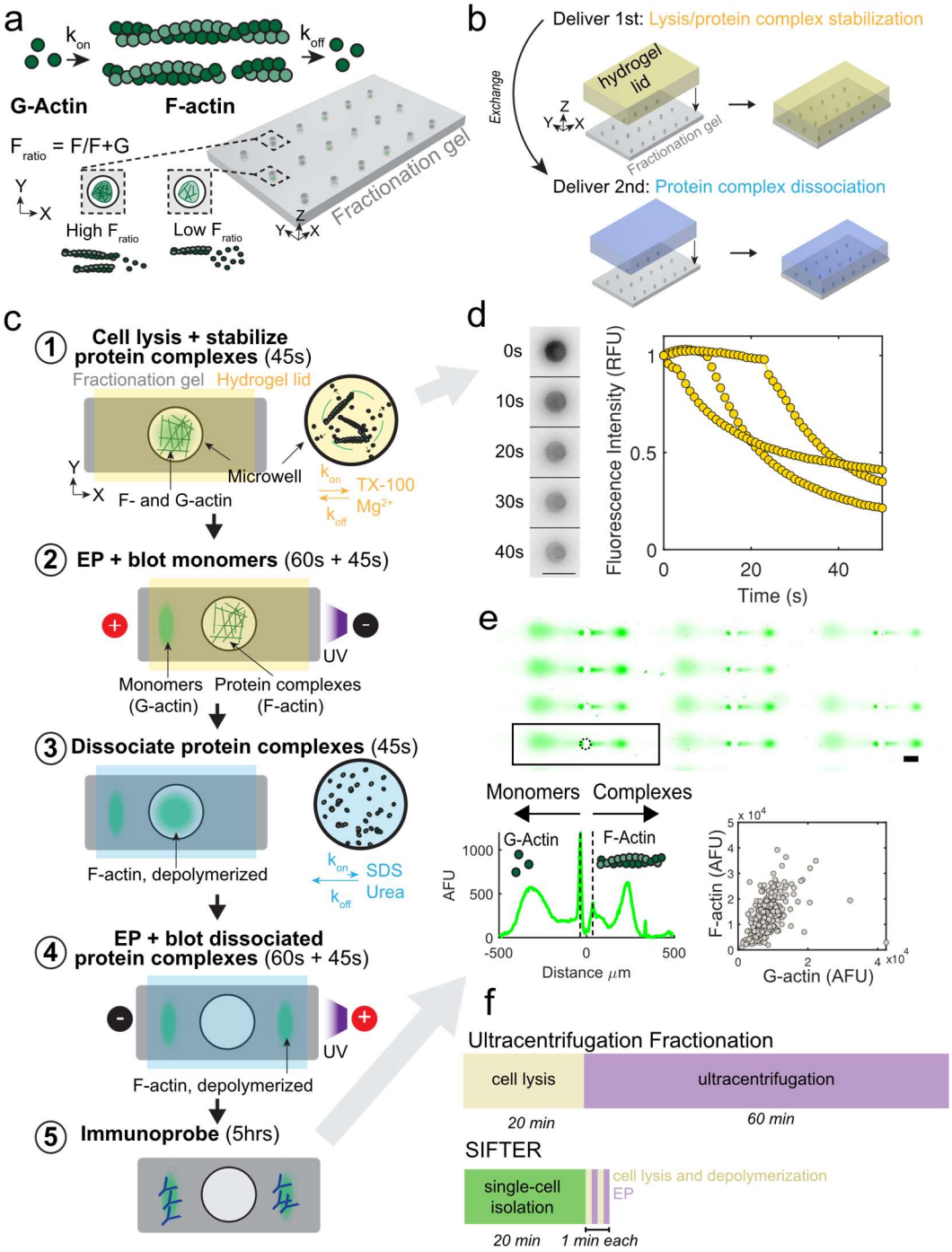

Figure 1: SIFTER integrates on-chip sample preparation, electrophoresis, and detection of F-actin complexes from hundreds of single cells. (a) Schematic of actin polymerization and depolymerization with rates, k_{on} and k_{off} from globular actin (G-actin, 42 kDa) and filamentous actin (F-actin; 4-100s of G-actin) in cells contained in a polyacrylamide fractionation gel. Cells are heterogeneous with low to high F-actin ratios (F_{ratio}) (b) Side-view schematic of hydrogel lid delivery of assay-stage optimized buffers to microwells in the fractionation gel. (c) The SIFTER assay comprises: 1) hydrogel lid delivery of protein complex-stabilizing lysis buffer to the array; 2) electrophoresis (EP) and UV-immobilization of monomers (e.g., G-actin) in the gel; 3) hydrogel lid delivery of protein-complex dissociation buffer; 4) EP of dissociated protein complexes (e.g., F-actin, depolymerized) in the opposite direction of monomers and UV immobilization; and 5) in-gel antibody immunoprobing. (d) Cell lysis monitoring: false-color fluorescence micrograph montage and quantification of

bioRxiv preprint doi: https://doi.org/10.1101/2020.09.12.294801; this version posted September 13, 2020. The copyright holder for this preprint (which was not certified by peer review) is the author/funder. All rights reserved. No reuse allowed without permission.

single MDA GFP-actin cells in microwells upon lysis with F-actin stabilization buffer (lyses cell but retains F-actin). Scale bar is 100 μm. Total fluorescence in the microwell normalized to initial in-well fluorescence as a function of lysis time for n=3 cells. (e) Immunoassay results: representative false-color micrograph of subset of the SIFTER array and intensity profiles of GFP F-actin and GFP G-actin from single MDA-MB-231 GFP-actin cells (scale bar is 100 μm). Microwell annotated with dashed line. Scatter plot depicts F- and G-actin peak area-under-the-curve from n = 276 single-cell protein complex separations from a single fractionation gel. (f) Schematic comparison of time scales for physical separation of protein complexes via bulk ultracentrifugation fractionation versus SIFTER. Single-cell isolation, unique to SIFTER, includes cell trypsinization and 10 minutes of passive gravity cell settling in the microwells.

To validate the selectivity to discern F- and G-actin states, we determined the gel composition needed to fractionate F-actin and directly observed EP of fluorescently labeled actin from single-cell lysates. The molecular mass cutoff for the gel depends on the total acrylamide concentration (%T). Based on native polyacrylamide gel EP[27,28], the SIFTER cutoff for an 8%T gel is ~740 kDa (Supplementary Fig. S1, Fig. 2a), or larger than 42 kDa G-actin, but smaller than an average ~2700 kDa F-actin. During EP of MDA-MB-231 GFP-actin cells (in which GFP is fused to both G- and F-actin), actin species indeed fractionate at the microwell edge (Fig. 2b). Within 45 s of EP, the G-actin Gaussian protein band completely injects 233 ± 11 μm into the polyacrylamide gel (with peak width sigma of 38.6 ± 5.3 μm, n=162; errors are standard deviations). We confirm the actin state of the species in the microwell by imaging EP of U2Os cells expressing RFP-Lifeact (a common marker for F-actin[14]). The microwell retains the F-actin complexes (Fig. 2c). We hypothesize two factors lead to no observed F-actin electromigration into the gel (including RFP-Lifeact bound dimers)[29]. First, small oligomers are a minor fraction of F-actin due to substantial dissociation rates[30]. Second, highly crosslinked filaments[31] remain enmeshed within the cytoskeleton even in lysed cells[32]. Thus, we confirm that SIFTER fractionates F-actin complexes from single cells. Size exclusion may fractionate other protein complexes by adjusting the %T, as >99% of individual proteins of the mammalian proteome are larger than the molecular mass cutoff of even a denser 10%T gel[33].

bioRxiv preprint doi: https://doi.org/10.1101/2020.09.12.294801; this version posted September 13, 2020. The copyright holder for this preprint (which was not certified by peer review) is the author/funder. All rights reserved. No reuse allowed without permission.

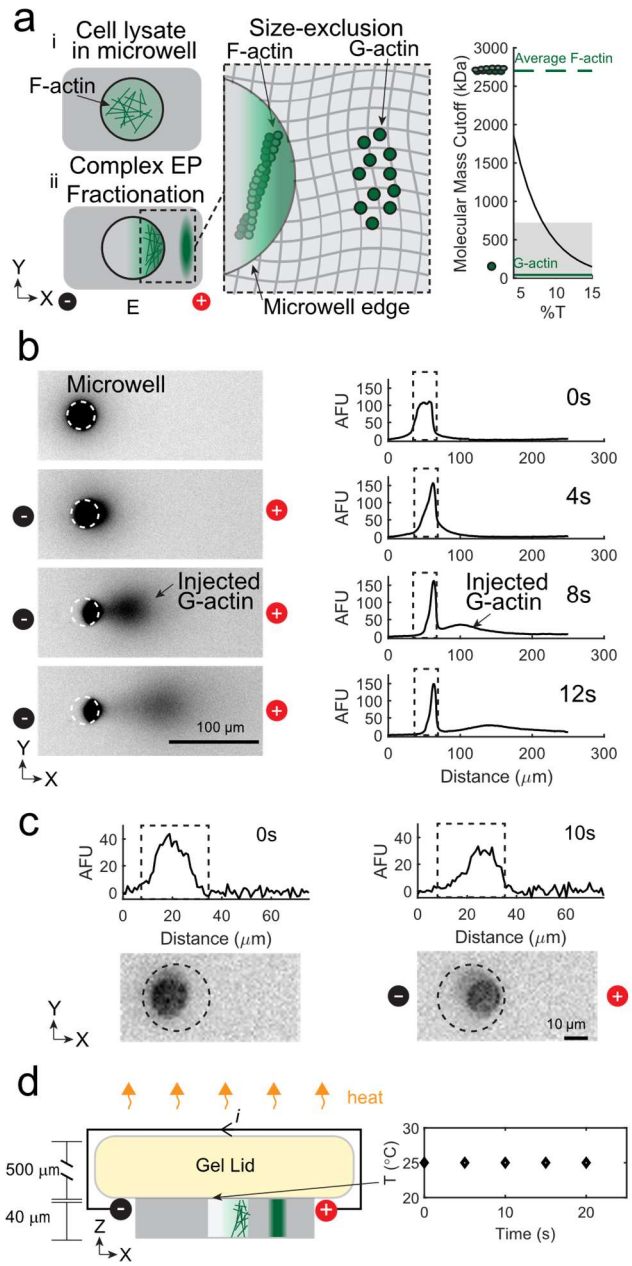

Figure 2: Size-based fractionation and efficient heat dissipation at the micro-scale provides molecular specificity to fractionate F-actin complexes from single cells. (a) Left: schematic of fractionation using polyacrylamide gel electrophoresis (EP) to separate F-actin complexes from G-actin monomers. Right: Estimated molecular mass cutoff as a function of gel density (%T). Shaded region is the molecular mass range of 99.9% of non-interacting protein species comprising the mammalian proteome, with notations indicating G-actin (42 kDa, solid green line) and average F-actin (~2700 kDa, dashed green line) molecular masses. (b) False-color fluorescence micrographs and corresponding intensity profiles during electrophoresis (30 V/cm) of MDA-MB-231 GFP-actin single-cell lysates in F-actin stabilization buffer; 76 ± 3% of the fluorescence remains in the microwell (n=4, error is standard deviation) (c) Intensity profiles (top) and false-color fluorescence micrographs of single RFP-Lifeact U2OS cells in microwells (dashed outline; only F-actin fluorescent) upon lysis in F-actin stabilization buffer. EP results in retention of F-actin complexes in the well. (d) Left: schematic of heating in the fractionation gel (gray) and gel lid (yellow) upon applying a current. Right: plot of temperature as function of electrophoresis time under the F-actin stabilization lysis buffer gel lid at 30V/cm.

bioRxiv preprint doi: https://doi.org/10.1101/2020.09.12.294801; this version posted September 13, 2020. The copyright holder for this preprint (which was not certified by peer review) is the author/funder. All rights reserved. No reuse allowed without permission.

We further validate SIFTER maintains F-actin complexes during fractionation without EP-induced temperature rise that would depolymerize F-actin complexes (e.g., above 45°C[34,35]). Electrical current passing through conductive buffer produces heat (Joule heating) during EP, which can increase temperature if not efficiently dissipated. The temperature difference, ΔT, between the surrounding medium and the conductor varies along the height axis, x, of the conductor: $\Delta T = E^2\sigma_c\left(\frac{H^2-x^2}{k}\right)$, where E is the electric field strength (V/m), σ_c is the buffer conductivity (S/m), H is the height and k is the thermal conductivity of the conductor (W/mK)[36]. Due to large temperature rises during EP in F-actin stabilization buffers containing $MgCl_2$ (σ_c ~1.3 mS/cm), E is limited to ~2-10 V/cm for 120-480 minutes in native slab gels[37], or ~18 V/cm in capillaries[37]. In SIFTER, the anticipated ΔT at 30 V/cm is only ~0.002°C (H~0.54 mm) versus ~7°C increase in a slab gel (H ~ 5 mm; Supplementary Figure S2). Indeed, we measure constant room temperature under the hydrogel lid during EP at 30 V/cm with SIFTER (Fig. 2d). Thus, we confirm SIFTER maintains F-actin complexes during fractionation that is ~100 times faster than in a slab gel and with 100-1000-fold higher sample throughput than a standard capillary (or comparable to automated capillary systems[38]).

Quantifying distributions of total actin and F_{ratio} across cells

To assess cellular heterogeneity, we asked: what are the statistical distributions of total actin and F_{ratio} across cells? Before answering these questions, we aimed to reduce run-to-run variation so we could compare distributions across replicates. We hypothesized we needed to measure the cells at a fixed time after preparing the single-cell suspension, as detachment lowers the level of cytoskeletal protein complexes[39–41]. With SIFTER we found F_{ratio} decreased by ~0.2 with increasing time left in suspension from 20 to 35 minutes (Kruskal-Wallis p-value < 0.0001, Dunn's post-hoc test for multiple comparisons p-values < 0.0001, Supplementary Fig. S3). In contrast, when we left cells in suspension for 10 minutes, F_{ratio} was indistinguishable across three replicate dishes of cells (split from a common source one day prior; Supplementary Fig. S4; Kruskal-Wallis p-value = 0.80; Dunn's post-hoc test for multiple comparisons p-values all > 0.89). In each of three replicates, we found total actin follows a gamma distribution, as expected based on transcriptional bursting (Supplementary Fig. S5, n = 138 to 217)[42]. For the first time, we find the F_{ratio} follows a normal distribution across cells (Supplementary Fig. S5). The normal F_{ratio} distribution measured with SIFTER suggests actin binding proteins stochastically regulate actin polymerization/depolymerization.

We aimed to evaluate the F_{ratio} distribution in cells expressing endogenous (not GFP-fused) actin, and found some immunoreagents yielded depolymerized F- but not G-actin immunoprobe signal (Supplementary Table S1, Supplementary Figure S6). Of note, a Fab fragment did yield G-actin immunoprobe signal in fibroblasts, while several full-length immunoreagents inconsistently detected G-actin in a subset of cells with F-actin signal. Lack of signal is not likely due to assay sensitivity, as actin is present at millions of copies of protein per cell[33] (while the in-gel immunoprobing limit-of-detection is ~27,000 copies of protein[20]). We instead hypothesize sterics may influence epitope availability to allow the Fab fragment to bind native G-actin immobilized to the gel but not full-length antibodies (~3-fold larger). Thus, we could discern differences in F-actin ratio distributions by cell type with concerted immunoprobe screening (Supplementary Figure S7).

bioRxiv preprint doi: https://doi.org/10.1101/2020.09.12.294801; this version posted September 13, 2020. The copyright holder for this preprint (which was not certified by peer review) is the author/funder. All rights reserved. No reuse allowed without permission.

SIFTER investigates cellular heterogeneity of F-actin complex-levels in response to drug treatment

We sought to quantify single-cell heterogeneity of F-actin complex-levels as quantitative assessment is needed for screening drugs targeting metastatic cell subpopulations[43]. In conventional imaging of F-actin with phalloidin (conjugated to a fluorophore), three factors pose a challenge to quantifying F-actin complex heterogeneity. First, phalloidin competes with both actin-binding proteins (e.g., cofilin)[17] and drugs (e.g., actin nucleating drug jasplakinolide, Jpk[18]). Second, phalloidin binds most but not all F-actin complexes *in vivo* (e.g., not Golgi-associated filaments)[44]. Third, optimal cell segmentation requires that cells are not in contact with one another[45], which limits quantification from tissues, and high-throughput analysis[45]. On the other hand, SIFTER is free from competitive binding or cell segmentation challenges.

We investigated two well-studied drugs with SIFTER (Figure 3): Jpk and Latrunculin A (LatA)[46]. Understanding Jpk effects on F-actin complexes is confounded by competitive binding with phalloidin and differing observations *in vivo* versus *in vitro*[47]. Jpk lowers the number of actin subunits at which k_{on} becomes appreciable, causing disordered aggregates[47]. Still, F-actin complex levels increase in certain cell types with Jpk treatment in the 0.1 - 1.0 μM range as determined by bulk ultracentrifugation[48,49]. With phalloidin staining of Jpk-treated BJ fibroblasts, we qualitatively observe shorter filaments and small aggregates. It is difficult to discern if competition with phalloidin obscures interpretation (Fig. 3a). SIFTER clearly yields a ~3.6-fold decrease in median F-actin (Mann-Whitney U-test p-value < 0.0001, Fig. 3b-c). To assess heterogeneity in SIFTER F-actin complex-levels across 100s of individual cells, we calculate the coefficient of quartile variation (CQV), a metric of variance accounting for skewed distributions[50], such as gamma-distributed protein expression[51]. The $CQV = \frac{Q_3 - Q_1}{Q_3 + Q_1}$, where Q_3 is the 75th percentile and Q_1 is the 25th percentile F-actin level. We find $CQV_{DMSO\ control,\ BJ}$ =0.46 and $CQV_{Jpk,\ BJ}$ =0.34 (subscripts refer to the treatment and cell type), meaning the drug effect is relatively uniform across the cell population.

LatA sequesters G-actin and reduces both F-actin complex-levels and the $F_{ratio,}$ as determined by phalloidin staining and bulk methods, respectiveley[46,52], but variation in cell response is unknown. After treatment with LatA, we phalloidin stained U2OS cells and observe decreased F-actin complex-fluorescence (Fig. 3a) in agreement with previous findings[53]. With SIFTER, we observe a statistically significant 2.7-fold decrease in the median F-actin complex-levels upon LatA treatment (Mann-Whitney P-value < 0.0001, Fig. 3d-e). Interestingly, LatA treatment also corresponds with an increase in F-actin CQV as $CQV_{LatA,\ U2OS}$ = 0.70 vs. $CQV_{DMSO\ control,\ U2OS}$ =0.42. Previously, phalloidin staining revealed a single F-actin complex-phenotype from hundreds of sparsely seeded cells treated with 250 nM LatA[54]. Here, the CQV increase upon LatA exposure suggests differential cell tolerance to LatA potentially due to either the almost ten-fold higher LatA concentrations utilized here, or the limitations of phalloidin staining. Thus, SIFTER circumvents competitive binding or cell segmentation challenges to quantify variation in drug effects on F-actin complexes at the single-cell level. The high $CQV_{LatA,\ U2OS}$ prompted us to further investigate cellular variation in response to LatA treatment.

bioRxiv preprint doi: https://doi.org/10.1101/2020.09.12.294801; this version posted September 13, 2020. The copyright holder for this preprint (which was not certified by peer review) is the author/funder. All rights reserved. No reuse allowed without permission.

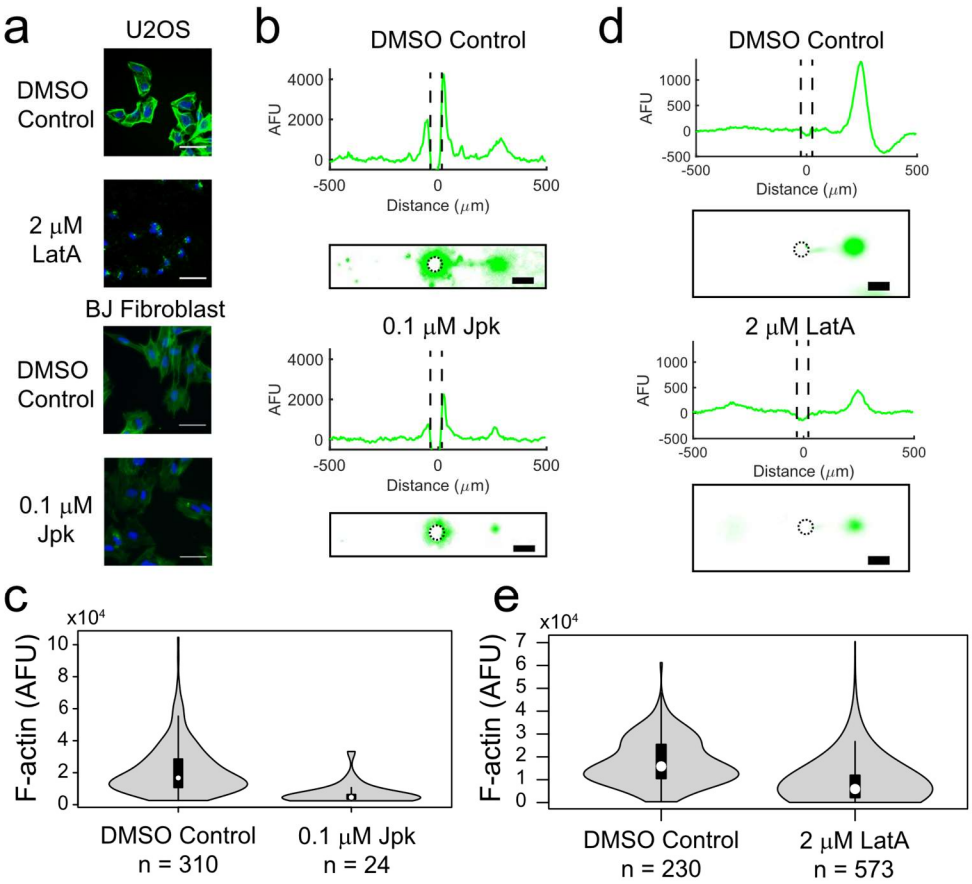

Figure 3: SIFTER quantifies cellular heterogeneity in F-actin complex-levels, avoiding competitive binding or cell segmentation challenges encountered with phalloidin staining. (a) False-color fluorescence micrographs of U2OS or BJ fibroblast cells fixed and stained with fluorescent phalloidin (F-actin, green) and Hoechst (nuclear stain, blue) after incubation with LatA (60 min) or Jpk (120 min). Scale bar is 50 μm. (b) False-color fluorescence micrographs and representative intensity profiles from SIFTER on single BJ fibroblast cells. Scale bar is 100 μm. Microwell is outlined with a dashed line in the intensity profile (c) Violin plot of F-actin levels quantified from two different SIFTER devices with the indicated total number of single cells. Medians are 16736 for control and 4601 for Jpk. Mann-Whitney U = 54791 with p-value < 0.0001. (d) False-color fluorescence micrographs and representative intensity profiles from performing SIFTER on single U2OS cells. Scale bar is 100 μm. (e) Violin plot of F-actin levels quantified from four different SIFTER devices with the indicated total number of single cells. Medians are 15840 for control and 5903 for LatA. Mann-Whitney U = 127440 with p-value < 0.0001.

Multiplexed cytoskeletal protein-complex quantification uncovers compensation for actin perturbation in subpopulations of cells

We asked two questions regarding Latrunculin A-induced cellular variation, recognizing that SIFTER could permit measurement of all three major cytoskeletal protein complexes simultaneously. First, we sought to understand if LatA yields differential expression of other cytoskeletal protein complexes. Second, we asked whether LatA induced unique cell subpopulations. The cytoskeletal protein complexes F-actin, microtubules (MT, of α- and β-tubulin subunits), and intermediate filaments (IF, of vimentin or keratin subunits) have both redundant and distinct functions in maintaining cytoskeletal integrity (Figure 4a). Such redundancy[55] yields increased IF to counteract F-actin destabilization of mesenchymal cells[56]

bioRxiv preprint doi: https://doi.org/10.1101/2020.09.12.294801; this version posted September 13, 2020. The copyright holder for this preprint (which was not certified by peer review) is the author/funder. All rights reserved. No reuse allowed without permission.

with another Latrunculin, LatB. Yet, quantification of cytoskeletal changes remains a challenge in single cells due to segmentation artifacts and low signal-to-noise ratio from immunohistochemistry and phalloidin staining[57,58]. SIFTER, in contrast, is compatible with MT and IF due to the relative stability of MT (depolymerization $t_{1/2}$ timescales of minutes[59]) and IF (subunit exchange ~10% over 7 hours[60]) and the similarity in protein complex-stabilizing buffers for each (Triton X-100 ~0.5-1%, pH ~6.7-7.4, and inclusion of 1 mM $MgCl_2$ for MT[19,61,62]).

To understand concerted effects of LatA drug treatment on F-actin, MT and IF, we performed SIFTER, and immunoprobed with antibodies for each (Figure 4b and Supplementary Figure S8). We observe correlation between the three protein complexes in the DMSO vehicle control cells (n = 92 single cells), with Spearman rank correlation $\rho = 0.66$ for MT vs. F-actin, $\rho = 0.64$ for F-actin vs. IF, and $\rho = 0.56$ for MT vs. IF (Supplementary Figure S9; $p < 0.01$ for each correlation). Despite correlation that suggests coordination of cytoskeletal protein-complex levels, agglomerative hierarchical clustering reveals cells with distinct patterns of protein-complex expression (e.g., groups A-F, Figure 4c).

Next, to elucidate whether any of the potential subpopulations shown in Figure 4c (e.g., groups A-F) were unique to the LatA-treatment, we adapted the GeneFishing method[63] for "CellFishing". Using a group of co-expressed cells as "bait", we attempt to "fish out" other cells from a candidate pool that present a similar protein complex-expression pattern to that of the bait cells. We do this through a semi-supervised clustering approach, coupled with sub-sampling to ensure robust discoveries. Here, groups of LatA-treated cells from hierarchical clustering that appear as unique phenotypes each define a set of "bait cells", and the DMSO control cells define the candidate pool. If a group of bait cells does not identify any cells with similar phenotypes in the DMSO control cells, we assume the phenotype is unique to the LatA-treated cell population. We found that bait groups A, B, E and F do not fish out DMSO control cells, while groups C and D are examples of baits that do (Figure 4d). Group A (~11% of LatA-treated cells) is characterized by elevated IF and MT in response to F-actin destabilization. Note, 7 bait cells in Group A (Figure 4d) form a tighter and more distant sub-group from the DMSO control cells. Groups B and F (~8% and 7% of cells respectively) only sees the counteracting increase in either MT or IF, but not both. Compensation for F-actin perturbation by MT and/or IF in subpopulations of cells suggests these cells are better equipped to maintain cytoskeletal integrity in response to stress. Groups C (~10% of LatA cells) and D (~16% of LatA cells) both fish out small numbers of DMSO control cells (~6% and 3% of the DMSO control cells, respectively) and thus represent phenotypes not exclusive to LatA treatment. We hypothesize Groups D and E with low F-actin, MT and IF, may be experiencing cytoskeletal collapse during apoptosis[64] (LatA IC_{50} is ~0.5 - 3.0 μM with 24-hr exposure in breast and lung cancer cells)[65]. Thus, SIFTER reveals subpopulations of cells with varying degrees of cytoskeletal integrity.

bioRxiv preprint doi: https://doi.org/10.1101/2020.09.12.294801; this version posted September 13, 2020. The copyright holder for this preprint (which was not certified by peer review) is the author/funder. All rights reserved. No reuse allowed without permission.

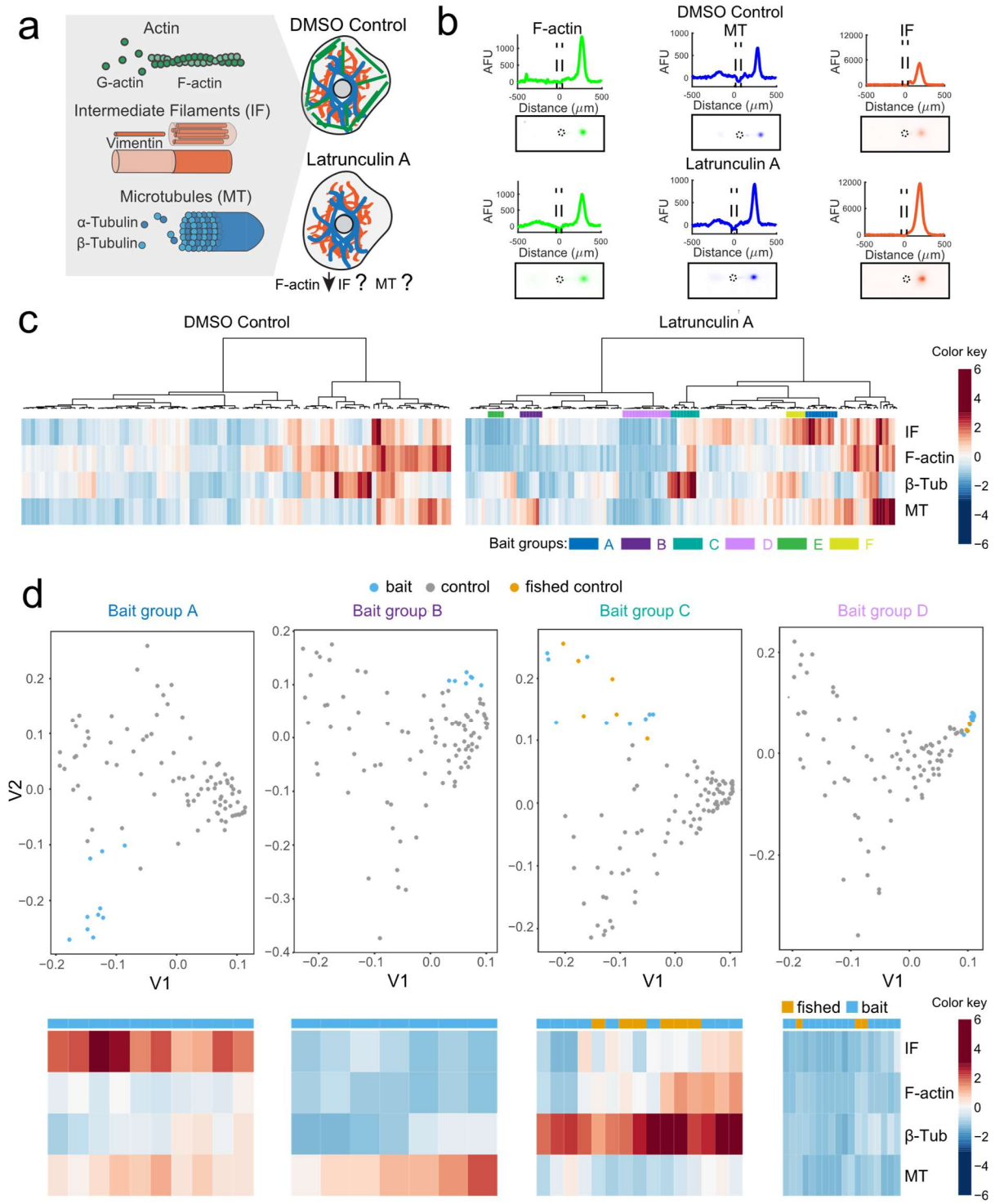

Figure 4: Multiplexed SIFTER detects subpopulations of cells with altered cytoskeletal protein complexes in response to F-actin destabilization. a) Schematic of the cell cytoskeleton composed of F-actin, intermediate filaments (IF) and microtubules (MT), and the unknown effects of Latrunculin A (LatA) on IF and MT. (b) Representative false-color fluorescence micrographs and intensity profiles from SIFTER. Monomeric proteins (e.g., β-Tubulin, β-Tub) are electrophoresed left of the microwell while F-actin, MT and IF are electrophoresed to the right of the microwell. Protein quantification is performed by peak area integration. Scale bar is 100 µm. (c) Heat maps with dendrograms from agglomerative hierarchical clustering with Euclidean distance metric and Ward linkage for U2OS cells incubated in DMSO (n = 92 cells, four SIFTER gels) or 2 µM Latrunculin A (LatA,

bioRxiv preprint doi: https://doi.org/10.1101/2020.09.12.294801; this version posted September 13, 2020. The copyright holder for this preprint (which was not certified by peer review) is the author/funder. All rights reserved. No reuse allowed without permission.

n = 134 cells, four SIFTER gels). Distinct sub-lineages used as bait groups A-F for CellFishing are shown with colored bars. Heatmap is standardized by row (mean at 0, and color gradations at units of standard deviation). (d) Spectral clustering projections and heatmaps depicting LatA treatment bait group cells (blue), DMSO control cells (grey) and fished out DMSO control cells (yellow).

Understanding cellular heterogeneity in actin distribution upon heat shock

To assess how a non-chemical stress perturbs (1) the F_{ratio} distribution and (2) F- and G-actin coordination, we apply SIFTER to the study of heat shock. Cytoskeletal reorganization is a hallmark of disease states[5], and protein-complex dysfunction is prominent in aging[66] and during cellular stress[67,68]. Cell stresses such as heat shock yields re-organization of F-actin in many, but not all cell types[69]. Indeed, with phalloidin staining, we observed a qualitative decrease in F-actin fluorescence of RFP-Lentiviral transformed MDA-MB-231 GFP-actin cells upon heat shock (Fig 5a).

For more nuanced characterization of the F_{ratio} distribution not possible with phalloidin staining, SIFTER reports the median F_{ratio} in the heat-shocked cells was similar to control cells (0.57 *vs.* 0.61, respectively; Mann-Whitney p-value is 0.0036, Fig. 5b-c). However, the interquartile range of the F_{ratio} in heat-shocked cells is nearly double that of control cells (0.16 *vs.* 0.09). We quantified the skew of the distribution with the Pearson's moment coefficient of skew $\overline{\mu_3} = \varepsilon\left[\left(\frac{X-\mu}{\sigma}\right)^3\right]$, where ε is the expectation operator, X is the random variable (here, F_{ratio}), μ is the distribution mean and σ is the standard deviation. We find $\bar{\mu}_3$ is 0.08 for the control data set, and -0.32 for the heat-shocked cells with skew towards increased G-actin levels (Fig. 5d).

To understand if increased G-actin corresponds with discoordination of F- and G-actin levels upon heat shock, we quantified Spearman ρ (for F- and G-actin level correlation). The Spearman ρ decreased from 0.82 for the control to 0.42 for heat-shocked cells. Together, we conclude that F-actin levels alone cannot reveal cytoskeletal integrity: the F_{ratio} distribution and Spearman ρ uncover differential stress response across the cell population.

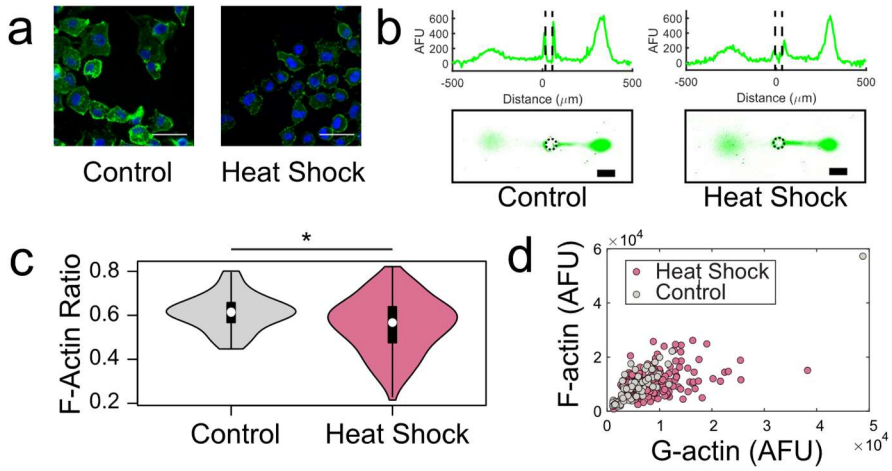

Figure 5: SIFTER quantifies actin distribution heterogeneity after heat-shock stress. (A) False-color fluorescence micrographs of adherent MDA-MB-231 GFP-actin cells with RFP-lentiviral transfection that were

bioRxiv preprint doi: https://doi.org/10.1101/2020.09.12.294801; this version posted September 13, 2020. The copyright holder for this preprint (which was not certified by peer review) is the author/funder. All rights reserved. No reuse allowed without permission.

fixed and stained for F-actin (phalloidin, green) and the nucleus (Hoechst, blue) with heat shock (45°C for 60 min) or 37°C control. Scale bar is 50 μm. (B) Representative false-color fluorescence micrographs and intensity profiles of GFP-actin EP fractionation from the specified single cells. Scale bar is 100 μm. (C) Violin plots of F-actin ratio (F/F+G) from SIFTER with n = 81 for the control (one SIFTER gel) and n = 188 for the heat shock condition (two SIFTER gels). Median F_{ratio} is 0.61 for control and 0.57 for heat shock. Mann-Whitney U = 12965 and the p-value is significant (*) at p = 0.0036. (D) Scatter plot of F versus G-actin. Spearman ρ = 0.82 for control and ρ = 0.42 for heat shock.

Discussion

SIFTER maintains multimeric protein complexes during fractionation to reveal monomer versus protein-complex states in single cells. We identify previously unknown cell subpopulations, such as the cluster with decreased F-actin, and compensatory increases in intermediate filaments and microtubules upon LatA treatment. Further, we found marked F- and G-actin dysregulation and variability upon heat shock. Our results present the intriguing possibility that SIFTER presents a more nuanced assessment of cytoskeletal integrity than phalloidin staining Thus, the assay unlocks the capability to assess single-cell heterogeneity in multimeric protein complexes, with broad applications across biology.

The range of detectable protein-complex sizes is set by a tradeoff between fractionation and immunoprobing. Denser gels compromise assay detection sensitivity because size-exclusion based partitioning lowers the in-gel antibody concentration during the immunoassay[20]. Fractionation in decrosslinkable gel[70] should allow isolation of up to 100s of the currently known mammalian protein complexes with masses of ~295 kDa or greater in a 12%T gel (~7 or more protein subunits[71], assuming each subunit has the average mammalian protein size of 375 amino acids[72], or mass of ~40 kDa).

For mechano-sensitive protein complexes within the cytoskeleton (e.g., stress fibers and focal adhesions), the fractionation gel functionality can be extended to also serve as a cell culture extracellular matrix. On-chip culture can assay adherent cells without trypsinization[73]. Thus SIFTER may evaluate single-cell regulation of actin in metastatic cancer cell subpopulations by quantifying dozens of actin binding proteins with increased multiplexing by stripping and re-probing[74]. Looking ahead, SIFTER could assist drug screens targeting diverse protein interactions underpinning invasive and heterogeneous cancer cells.

Online Methods

Chemicals: Tetramethylethylenediamine (TEMED, T9281), 40% T, 3.4% C acrylamide/bis-acrylamide (29:1) (A7802), N,N,N′,N′-, ammonium persulfate (APS, A3678), sodium deoxycholate (NaDOC, D6750), sodium dodecyl sulfate (SDS, L3771), bovine serum albumin (BSA, A7030), dithioerythritol (DTE, D8255), triton X-100 (X100), urea (U5378), β-Mercaptoethanol (M3148), anhydrous magnesium chloride ($MgCl_2$, 814733) and dimethylsulfoxide (DMSO, D2438) were acquired from Sigma Aldrich. An Ultrapure Millipore filtration system provided deionized water (18.2 MΩ). PharmAgra Laboratories custom-synthesized N-[3-[(3-Benzoylphenyl)- formamido] propyl] methacrylamide (BPMAC). Phosphate buffered saline was purchased from VWR (10X PBS, 45001−130). Tris glycine (10X) buffer was obtained from Bio-Rad (25 mM Tris, pH 8.3; 192 mM glycine, #1610734). Petroleum jelly (Cumberland Swan Petroleum Jelly, cat. no. 18−999−1829). Tris-HCl was obtained from Fisher Scientific (1M, pH = 7.5; Corning MT46030CM), while 0.5 M Tris-HCl, pH 6.8 was purchased from

bioRxiv preprint doi: https://doi.org/10.1101/2020.09.12.294801; this version posted September 13, 2020. The copyright holder for this preprint (which was not certified by peer review) is the author/funder. All rights reserved. No reuse allowed without permission.

Teknova (T1568). Photoinitiator 2,2-Azobis(2-methyl-N-(2-hydroxyethyl) propionamide) (VA-086) was acquired from FujiFilm Wako Pure Chemical Corporation. Gel Slick was purchased from Lonza (#50640). Tris Buffered Saline with Tween 20 (TBST-10X) was procured from Cell Signaling Technology (9997S). Paraformaldehyde (4% EM grade) was purchased from Electron Microscopy Sciences (157-4).

Cell culture: All cell lines were authenticated by short tandem repeat profiling by the UC Berkeley Cell Culture facility and tested negative for mycoplasma. Naive U2OS cells were purchased from the UC Berkeley Cell Culture Facility. BJ fibroblasts were provided by the Dillin lab. U2OS RFP-Lifeact cells were previously generated by the Kumar lab[75] at UC Berkeley, and kindly provided for this study. MDA-MB-231 GFP-actin cells were kindly provided by the Drubin lab at UC Berkeley. BJ fibroblasts and U2OS (RFP-Lifeact and naive) cells were maintained in DMEM (11965, ThermoFisher Scientific) supplemented with 10% FBS (100-106, GeminiBio), 1% penicillin/streptomycin (15140-122, ThermoFisher Scientific), and 1% non-essential amino acids (11140-050, ThermoFisher Scientific), while MDA-MB-231 GFP-actin cells were maintained in the same media minus the 1% non-essential amino acids. All cells were cultivated in a humidified incubator in 5% CO_2 kept at 37 °C. Cells were sub-cultured at ~80% confluency and detached with 0.05% Trypsin-EDTA (Gibco #25300-054) for 3 minutes. Each SIFTER assay was performed on a distinct single-cell suspension.

Generation of RFP-Lenti MDA-MB-231 GFP-Actin cells: MDM-MB-231 GFP-actin cells were a kind gift from the laboratory of Dr. David Drubin. Genome editing was performed at the genomic locus by integrating TagGFP (see Supplementary Methods) at the genomic locus for *ACTB*. Verification of genome editing was performed via standard PCR and sequencing. Briefly, DNA was collected from cells using the Qiagen DNeasy Blood and Tissue Kit (69506) as per manufacturer's guidelines. 100 ng of genomic DNA was used for PCR using forward primer 5'GGACTCAAGGCGCTAACTGC3' and reverse primer 5' GGTACTTCAGGGTGAGGATGCC3'. Sequencing was performed using standard sanger sequencing using primer 5'GCTTCCTTTGTCCCCAATCTGG3'. A schematic for genome editing is provided in Fig. S10. MDA-MB-231 GFP-actin cells were infected with lentivirus containing CD510B-1_pCDH-CMV-MCS-ED1-Puro (SystemBio) modified to carry TagRFP (see Supplementary Methods) under the CMV promoter.

SIFTER assay: Buffers and gel lid incubation: F-actin stabilization lysis buffer used was 10 mM Tris-HCl, 1% Triton X-100, 2 mM $MgCl_2$, and 0.5 mM DTE (titrated to pH=7.4). The DTE was added at the time of a given experiment. The depolymerization buffer was prepared as a 1.56x RIPA buffer such that upon addition of 8 M urea, the final buffer composition was 0.5x Tris glycine, 0.5% SDS, 0.25% sodium deoxycholate, 0.1% Triton X-100, 8 M urea, pH=8.3. Urea was added fresh at the time of the experiment and allowed to dissolve at 75°C. Hydrogel lids (15%T, 3.3% C) were photopolymerized as previously described between Gel Slick-coated glass plates offset with a 500 µm spacer[76]. Hydrogel lids were incubated overnight at 4°C in either the F-actin stabilization or the depolymerization buffer (before urea or DTE addition). Upon complete preparation of the urea-containing depolymerization buffer, the buffer was introduced to the gel lids in a water bath set to 75 °C and incubated for ~30 minutes before beginning the experiments. F-actin stabilization buffers and gel lids were kept at room temperature. Gel lids and buffers were only stored for up to 2 weeks, and buffer solution was never re-used.

bioRxiv preprint doi: https://doi.org/10.1101/2020.09.12.294801; this version posted September 13, 2020. The copyright holder for this preprint (which was not certified by peer review) is the author/funder. All rights reserved. No reuse allowed without permission.

Polyacrylamide fractionation gels (8%T and 3.3%C with 3 mM BPMAC incorporated) were polymerized on SU-8 micro-post molds as described elsewhere[77]. Trypsinized cells were introduced to the microwell array in 1X PBS solution for passive gravity settling. Trypsinization was performed for 3 minutes at 37°C, and cells in PBS (10010049, Thermo Fisher Scientific, pH=7.4, magnesium and calcium free) settled in the microwell array for 10 minutes. Each replicate experiment was run with a different 1-cm petri dish of freshly trypsinized cells in suspension.

For the fractionation separation, the fractionation gel device was pre-incubated in 10 mM Tris-HCl (pH=7.5) briefly before the glass slide was adhered to the surface of a custom 3D-printed EP chamber with petroleum jelly. A custom heater with a 12V PTC ceramic heating element (ELE147, Bolsen Tech) and PID temperature controller (ITC-106VH, Inkbird) was interfaced to the bottom surface of the EP chamber. The F-actin stabilization hydrogel lid was then applied to the array and cell lysis proceeded for 45s before the electric field was applied (30 V/cm, 45s for 42 kDa actin in U2OS or BJ fibroblasts, or 60s for 69 kDa GFP-actin from the GFP-actin cells; Bio-Rad Powerpac basic power supply). Proteins were blotted, or bound to the fractionation gel, by UV-induced covalent immobilization to the BPMAC incorporated in the fractionation gel (Lightningcure LC5, Hamamatsu, 100% power, 45 s). The electrode terminals were reversed, and the hydrogel lid was exchanged with depolymerization buffer gel hydrogel lid for 45s. EP was performed for the same duration in the opposite direction before a final UV photo-immobilization step (same UV power and duration). The glass slide was peeled from the EP chamber, and the fractionation gel was washed in 1X TBST for at least 30 min to overnight prior to immunoprobing.

Immunoprobing was performed as previously described[77], utilizing a rabbit anti-GFP antibody for GFP-actin (Abcam Ab290), mouse anti-actin monoclonal antibody (Millipore MAB1501 for BJ fibroblasts), rabbit anti-actin polyclonal antibody (Cytoskeleton Inc. AAN01), rhodamine-labeled anti-actin Fab (Biorad 12004164 for BJ fibroblasts), rabbit anti-actin monoclonal antibody (Abcam Ab 218787 for U2OS cells), mouse anti-vimentin monoclonal antibody (Abcam Ab8978) and rabbit anti-β-tubulin monoclonal antibody (Abcam Ab6046). Gels were incubated with 50 µl of 1:10 dilution of the stock primary antibody in TBST for two hours and then washed 2x for 30 minutes in 1X TBST. Donkey Anti-Rabbit IgG (H+L) Cross-Adsorbed Secondary Antibody, Alexa Fluor 647-labeled (A31573, Thermo Fisher Scientific), Donkey Anti-Mouse IgG (H+L) Cross-Adsorbed Secondary Antibody, Alexa Fluor 555-labeled (A31570, Thermo Fisher Scientific) and Donkey Anti-Mouse IgG (H+L) Cross-Adsorbed Secondary Antibody, Alexa Fluor 647-labeled (A31571, Thermo Fisher Scientific) were used at a 1:20 dilution in TBST for a one-hour incubation after 5 minutes of centrifugation at 10,000 RCF. Two more 30-min TBST washes were performed prior to drying the gels in a nitrogen stream and imaging with a laser microarray scanner (Genepix 4300A, Molecular Devices). When immunoprobing with rhodamine-labeled anti-actin Fab, 1:5 dilutions were used and immunoprobing completed after the two-hour Fab incubation and two 30-minute washes in TBST. For multiplexed analysis of actin, vimentin and β-tubulin protein complexes, actin and vimentin were immunoprobed together, the gels were chemically stripped[77] and then re-probed for β-tubulin. Chemical stripping was performed for at least one hour at 55°C. Gels were briefly rinsed in fresh 1x TBST three times and then washed in 1x TBST for at least one hour prior to re-probing.

bioRxiv preprint doi: https://doi.org/10.1101/2020.09.12.294801; this version posted September 13, 2020. The copyright holder for this preprint (which was not certified by peer review) is the author/funder. All rights reserved. No reuse allowed without permission.

Images were analyzed as described elsewhere[77]. Briefly, the images were median filtered utilizing the "Remove Outliers" macro in Fiji (pixel radius=2 and threshold=50 AFU). The images were then segmented, intensity profiles were generated for each separation lane by was fit to a Gaussian curve. For fits with an R^2>0.7 and peaks with an SNR>3, user-based quality control is performed, and area under the curve is calculated within two peak widths from the center on the background subtracted profile. Image analysis was performed in MATLAB R2019b.

Fluorescence imaging of cells in microwells, lysis and EP: Imaging was performed via time-lapse epi-fluorescence microscopy on an Olympus IX50 inverted epifluorescence microscope. The microscope was controlled using Metamorph software (Molecular Devices) and images were recorded with a CCD camera (Photometrics Coolsnap HQ2). The imaging setup included a motorized stage (ASI), a mercury arc lamp (X-cite, Lumen Dynamics) and an XF100-3 filter for GFP (Omega Optical) and an XF111-2 filter for RFP (Omega Optical). Imaging was performed with a 10× magnification objective (Olympus UPlanFLN, NA 0.45) and 900 ms exposures with 1s intervals with U2OS RFP-Lifeact, and 2s exposure with 2s intervals with MDA-MB-231 GFP-actin (1x pixel binning). Exposure times were lowered for lysis imaging to 600 ms.

F-actin cell staining with phalloidin and Latrunculin A and Jasplakinolide drug treatment: Latrunculin A (Cayman Chemicals 10010630) was dissolved in DMSO as a 2 mM stock solution and stored at -20 °C until use. Jasplakinolide (Millipore-Sigma, 420107) was reconstituted in DMSO and stored at -20 °C for up to 3 months. Cells were incubated in the drug solution at the concentration and for the time listed in the main text. The DMSO control cells were exposed to 0.1% DMSO in cell culture media for the same time as the drug treated cells. Cells were fixed with 3.7% paraformaldehyde in 1X PBS (10 minutes at room temperature), and permeabilized with 0.1% Triton X-100 (for 5 minutes at room temperature and stained with Alexa Fluor 647-labeled phalloidin (20 minutes at room temperature, ThermoFisher Scientific, A22287).

Heat shock treatment of cells: MDA-MB-231 GFP-actin RFP-lenti cells were incubated at 45 °C (VWR mini incubator, 10055-006) for 1-hour prior trypsinization and gravity settling in the fractionation gel.

Statistical analysis: Mann-Whitney test (with U test statistic) and Kruskal-Wallis test with post-hoc Dunn's test (Chi-squared test statistic), Spearman rank correlations, and QQ-plot generation with normal and gamma distributions were performed using pre-existing functions in MATLAB 2019b. All tests were two-sided. All boxplots include a centerline for the median, boxes at the 25th and 75th percentile and whiskers that extend to all data points. Violin plots were generated in RStudio (Version 0.99.903) using the library "Vioplot". The boxplot within the kernel density plot displays boxes at the 25th and 75th percentile, a point at the median, and whiskers that extend 1.5-times the box length.

Cell Fishing clustering analysis: Standardization is by row for both the LatA treated and DMSO control data sets (expression level, or Gaussian protein peak AUC, for each protein complex) with the mean at 0 and standard deviation of 1. Initial agglomerative hierarchical clustering was performed separately for the LatA treated and DMSO control data sets utilizing Euclidean distances, and the Ward linkage

bioRxiv preprint doi: https://doi.org/10.1101/2020.09.12.294801; this version posted September 13, 2020. The copyright holder for this preprint (which was not certified by peer review) is the author/funder. All rights reserved. No reuse allowed without permission.

criterion (R version 3.6.1, NMF package / MATLAB 2019b, Statistics and Machine Learning Toolbox). Distinct sub-clusters in the LatA treated data were further inspected as "bait" groups of cells inspired by the GeneFishing method described elsewhere[63] . We conducted an analogous analysis to GeneFishing, which we call "Cell Fishing". Candidate cells from the DMSO control data sets were randomly split into subsamples of 23-33 cells, and each subsample was pooled together with the "bait" cells to form a sub-dataset. Semi-supervised clustering is applied to each sub-dataset using spectral analysis and a clustering algorithm based on the EM-fitted mixture Gaussian of two components model[78] (R version 3.6.1, mclust package). The subsampling protocol was repeated 3000 times for a given "bait" set, and cells were considered "fished out" if they had a capture frequency rate of 0.99 or higher, as what is done in the GeneFishing paper[63] .

Acknowledgements
This work was supported in part by the Office of the Assistant Secretary of Defense for Health Affairs under Award No. W81XWH-16-1-0002 (PI: Herr). The authors share their own conclusions and interpretation, which are not inherently endorsed by the Department of Defense. Other support includes: NSF Graduate Fellowship DGE1106400 (J.V.), Society of Lab Automation and Screening Graduate Education Fellowship (J.V.), NIH K99 (1K99AG065200-01A1, R.H.-S.), NSF CAREER CBET1056035 (A.E.H.), NIH R01CA203018 (A.E.H.), NIH R01AG055891-01 (A.D.) and Howard Hughes Medical Institute (A.D.). We thank the laboratories of David Drubin and Sanjay Kumar at UC Berkeley for providing the GFP-actin MDA-MB-231 and U2OS RFP-Lifeact edited cells, respectively.

Availability of code: MATLAB functions to analyze protein expression levels from SIFTER gel images are available on Github (https://github.com/herrlabucb/summit). The GeneFishing algorithm for Python is also available on Github (https://github.com/tomwhoooo/GeneFishingPy).

Availability of data: The data generated for this study are available in the Figshare repository with DOI: https://doi.org/10.6084/m9.figshare.c.5115779.v1

Author Contributions
J.V., L.L.H, R.H.-S. and A.E.H. designed the experiments. J.V. and L.L.H. performed SIFTER assay and analysis, and phalloidin staining of cells. C.K.T. provided cell culture and cell line modification support. Y.Z. and H.H. designed and performed Cell Fishing clustering analysis. All authors wrote the manuscript.

Competing Financial Interests
J.V. and A.E.H. are inventors on single-cell protein separation intellectual property, which may result in licensing royalties.

References:
1. De Las Rivas, J. & Fontanillo, C. Protein–Protein Interactions Essentials: Key Concepts to Building and Analyzing Interactome Networks. *PLoS Comput. Biol.* **6**, e1000807 (2010).
2. Condeelis, J. How is actin polymerization nucleated in vivo? *Trends Cell Biol.* **11**, 288–293 (2001).
3. Wegner, A. Treadmilling of actin at physiological salt concentrations. *J. Mol. Biol.* **161**, 607–615 (1982).
4. Masai, J., Ishiwata, S. & Fujime, S. Dynamic light-scattering study on polymerization process of muscle actin. *Biophys. Chem.* **25**, 253–269 (1986).

bioRxiv preprint doi: https://doi.org/10.1101/2020.09.12.294801; this version posted September 13, 2020. The copyright holder for this preprint (which was not certified by peer review) is the author/funder. All rights reserved. No reuse allowed without permission.

5. Rao, K. M. K. & Cohen, H. J. Actin cytoskeletal network in aging and cancer. *Mutat. Res.* **256**, 139–148 (1991).
6. Senderowicz, A. M. *et al.* Jasplakinolide's inhibition of the growth of prostate carcinoma cells in vitro with disruption of the actin cytoskeleton. *J. Natl. Cancer Inst.* **87**, 46–51 (1995).
7. Donnelly, D. P. *et al.* Best practices and benchmarks for intact protein analysis for top-down mass spectrometry. *Nat. Methods* **16,** 587-594 (2019).
8. Budnik, B., Levy, E., Harmange, G. & Slavov, N. SCoPE-MS: Mass spectrometry of single mammalian cells quantifies proteome heterogeneity during cell differentiation. *Genome Biol.* **19**, 1–12 (2018).
9. Zhu, Y. *et al.* Nanodroplet processing platform for deep and quantitative proteome profiling of 10 – 100 mammalian cells. *Nat. Commun.* **9**, 882 (2018).
10. Söderberg, O. *et al*. Direct observation of individual endogenous protein complexes in situ by proximity ligation. *Nat. Methods* **3**, 995–1000 (2006).
11. Roy, R., Hohng, S. & Ha, T. A practical guide to single-molecule FRET. *Nat. Methods* **5**, 507–516 (2008).
12. Kamiyama, D. *et al.* Versatile protein tagging in cells with split fluorescent protein. *Nat. Commun.* **7,** 11046 (2016).
13. Melak, M., Plessner, M. & Grosse, R. Actin visualization at a glance. *J. Cell Sci.* **130**, 525–530 (2017).
14. Riedl, J. *et al.* Lifeact: a versatile marker to visualize F-actin. *Nat. Methods* **5**, 605–7 (2008).
15. Spracklen, A. J., Fagan, T. N., Lovander, K. E. & Tootle, T. L. The pros and cons of common actin labeling tools for visualizing actin dynamics during Drosophila oogenesis. *Dev. Biol.* **393**, 209–226 (2014).
16. Cooper, J. A. Effects of cytochalasin and phalloidin on actin. *J. Cell Biol.* **105**, 1473–1478 (1987).
17. Mcgough, A., Pope, B., Chiu, W. & Weeds, A. Cofilin Changes the Twist of F-Actin: Implications for Actin Filament Dynamics and Cellular Function. *J. Cell Biol.* **138**, 771–781 (1997).
18. Bubb, M. R., Senderowicz, A. M., Sausville, E. A., Duncan, K. L. & Korn, E. D. Jasplakinolide, a cytotoxic natural product, induces actin polymerization and competitively inhibits the binding of phalloidin to F-actin. *J. Biol. Chem.* **269**, 14869–71 (1994).
19. Heacock, C. S. & Bamburg, J. R. The quantitation of G- and F-actin in cultured cells. *Anal. Biochem.* **135**, 22–36 (1983).
20. Kang, C.-C. *et al.* Single cell–resolution western blotting. *Nat. Protoc.* **11**, 1508–1530 (2016).
21. Bray, D. *Cell Movements: From Molecules to Motility*. *Garland Science, 2nd Edition* (2000).
22. Cano, M. L., Lauffenburger, D. A. & Zigmond, S. H. Kinetic analysis of F-actin depolymerization in polymorphonuclear leukocyte lysates indicates that chemoattractant stimulation increases actin filament number without altering the filament length distribution. *J. Cell Biol.* **115**, 677–687 (1991).
23. Bray, D. & Thomas, C. Unpolymerized actin in fibroblasts and brain. *J. Mol. Biol.* **105**, 527–544 (1976).
24. Ujfalusi-Pozsonyi, K. *et al.* The effects of detergents on the polymerization properties of actin. *Cytom. Part A* **77A**, 447-456 (2010).
25. Leaist, D. G. A moving-boundary technique for the measurement of diffusion in liquids. triton X-100 in water. *J. Solution Chem.* **20**, 187–197 (1991).
26. Heinz, L. S. *et al.* Strong fascin expression promotes metastasis independent of its F-actin bundling activity. *Oncotarget* **8**, 110077–110091 (2017).
27. Rodbard, D., Kapadiia, G. & Chrambach, A. Pore gradient electrophoresis. *Anal. Biochem.* **157**, 135–157 (1971).
28. Wittig, I., Beckhaus, T., Wumaier, Z., Karas, M. & Schägger, H. Mass estimation of native proteins by blue native electrophoresis: Principles and practical hints. *Mol. Cell. Proteomics* **9**, 2149–2161 (2010).
29. Kumari, A., Kesarwani, S., Javoor, M. G., Vinothkumar, K. R. & Sirajuddin, M. Structural insights into filament recognition by cellular actin markers. *EMBO J.* **e104006**, 1–13 (2020).
30. Pollard, T. D. & Cooper, J. A. Actin, a central player in cell shape and movement. *Science (80-.).* **326**, 1208–1212 (2009).
31. dos Remedios, C. G. *et al.* Actin binding proteins: regulation of cytoskeletal microfilaments. *Physiol. Rev.* **83**, 433–73 (2003).
32. Cano, M. L., Cassimeris, L., Fechheimer, M. & Zigmond, S. H. Mechanisms Responsible for F-actin Stabilization after Lysis of Polymorphonuclear Leukocytes. *J. Cell Biol.* **116,** 1123-1134 (1992).
33. Li, J. J., Bickel, P. J. & Biggin, M. D. System wide analyses have underestimated protein abundances and the importance of transcription in mammals. *PeerJ* **2**, e270 (2014).

bioRxiv preprint doi: https://doi.org/10.1101/2020.09.12.294801; this version posted September 13, 2020. The copyright holder for this preprint (which was not certified by peer review) is the author/funder. All rights reserved. No reuse allowed without permission.

34. Turi, A. Lu, R.C. Lin, P.-C. Effect of heat on the microtubule disassembly and its relationship to body temperatures. *Biochem. Biophys. Res. Commun.* **100**, 584–590 (1981).
35. Wendel, H. & Dancker, P. Kinetics of actin depolymerization: influence of ions, temperature, age of F-actin, cytochalasin B and phalloidin. *Biochim. Biophys. Acta - Protein Struct. Mol. Enzymol.* **873**, 387–396 (1986).
36. Cifuentes, A. & Poppe, H. Rectangular capillary electrophoresis: Some theoretical considerations. *Chromatographia* **39**, 391–404 (1994).
37. Borejdo, J. & Burlacu, S. Distribution of actin filament lengths and their orientation measured by gel electrophoresis in capillaries. *J. Muscle Res. Cell Motil.* **12**, 394–407 (1991).
38. Dickinson, A. J., Armistead, P. M. & Allbritton, N. L. Automated Capillary Electrophoresis System for Fast Single-Cell Analysis. *Anal. Chem.* **85**, 4797–4804 (2013).
39. Bereiter-Hahn, J., Lück, M., Miebach, T., Stelzer, H. K. & Vöth, M. Spreading of trypsinized cells: cytoskeletal dynamics and energy requirements. *J. Cell Sci.* **96 (Pt 1)**, 171–88 (1990).
40. Knowles, G. C. & McCulloch, C. A. Simultaneous localization and quantification of relative G and F actin content: optimization of fluorescence labeling methods. *J. Histochem. Cytochem.* **40**, 1605–12 (1992).
41. Clark, E. A., King, W. G., Brugge, J. S., Symons, M. & Hynes, R. O. Integrin-mediated signals regulated by members of the rho family of gtpases. *J. Cell Biol.* **142**, 573–586 (1998).
42. Cai, L., Friedman, N. & Xie, X. S. Stochastic protein expression in individual cells at the single molecule level. *Nature* **440**, 358–62 (2006).
43. Fife, C. M., McCarroll, J. A. & Kavallaris, M. Movers and shakers: Cell cytoskeleton in cancer metastasis. *British Journal of Pharmacology* **171**, 5507–5523 (2014).
44. Belin, B. J., Goins, L. M. & Mullins, R. D. Comparative analysis of tools for live cell imaging of actin network architecture. *Bioarchitecture* **4**, 189–202 (2014).
45. Zonderland, J., Wieringa, P. & Moroni, L. A quantitative method to analyse F-actin distribution in cells. *MethodsX* **6**, 2562–2569 (2019).
46. Coué, M., Brenner, S. L., Spector, I. & Korn, E. D. Inhibition of actin polymerization by latrunculin A. *FEBS Lett.* **213**, 316–318 (1987).
47. Bubb, M. R., Spector, I., Beyer, B. B. & Fosen, K. M. Effects of jasplakinolide on the kinetics of actin polymerization. An explanation for certain in vivo observations. *J. Biol. Chem.* **275**, 5163–70 (2000).
48. Diamond, M. I. *et al.* Subcellular localization and Ser-137 phosphorylation regulate tumor-suppressive activity of profilin-1. *J. Biol. Chem.* **290**, 9075–86 (2015).
49. Kiuchi, T., Nagai, T., Ohashi, K. & Mizuno, K. Measurements of spatiotemporal changes in G-actin concentration reveal its effect on stimulus-induced actin assembly and lamellipodium extension. *J. Cell Biol.* **193**, 365–80 (2011).
50. Bonett, D. G. Confidence interval for a coefficient of quartile variation. *Comput. Stat. Data Anal.* **50**, 2953–2957 (2006).
51. Taniguchi, Y. *et al.* Quantifying E. coli proteome and transcriptome with single-molecule sensitivity in single cells. *Science* **329**, 533–8 (2010).
52. Lyubchenko, T. a, Wurth, G. a & Zweifach, A. The actin cytoskeleton and cytotoxic T lymphocytes: evidence for multiple roles that could affect granule exocytosis-dependent target cell killing. *J. Physiol.* **547**, 835–847 (2003).
53. Vindin, H., Bischof, L., Gunning, P. & Stehn, J. Validation of an algorithm to quantify changes in actin cytoskeletal organization. *J. Biomol. Screen.* **19,** 354-368 (2014).
54. Bryce, N. S. *et al.* High-Content Imaging of Unbiased Chemical Perturbations Reveals that the Phenotypic Plasticity of the Actin Cytoskeleton Is Constrained. *Cell Syst.* **9**, 496–507 (2019).
55. Huber, F., Boire, A., López, M. P. & Koenderink, G. H. Cytoskeletal crosstalk: When three different personalities team up. *Curr. Opin. Cell Biol.* **32**, 39–47 (2015).
56. Chang, T. H. *et al.* The effects of actin cytoskeleton perturbation on keratin intermediate filament formation in mesenchymal stem/stromal cells. *Biomaterials* **35**, 3934–3944 (2014).
57. Sum, C. S. *et al.* Establishing a High-content Analysis Method for Tubulin Polymerization to Evaluate Both the Stabilizing and Destabilizing Activities of Compounds. *Curr. Chem. Genomics Transl. Med.* **8**, 16–26 (2014).
58. Xiao, X., Geyer, V. F., Bowne-Anderson, H., Howard, J. & Sbalzarini, I. F. Automatic optimal filament segmentation with sub-pixel accuracy using generalized linear models and B-spline level-sets. *Med. Image*

bioRxiv preprint doi: https://doi.org/10.1101/2020.09.12.294801; this version posted September 13, 2020. The copyright holder for this preprint (which was not certified by peer review) is the author/funder. All rights reserved. No reuse allowed without permission.

Anal. **32**, 157–172 (2016).
59. Caudron, N., Valiron, O., Usson, Y., Valiron, P. & Job, D. A reassessment of the factors affecting microtubule assembly and disassembly in vitro. *J. Mol. Biol.* **297**, 211–220 (2000).
60. Nöding, B., Herrmann, H. & Köster, S. Direct Observation of Subunit Exchange along Mature Vimentin Intermediate Filaments. *Biophys. J.* **107**, 2923–2931 (2014).
61. Battaglia, R. A., Kabiraj, P., Willcockson, H. H., Lian, M. & Snider, N. T. Isolation of intermediate filament proteins from multiple mouse tissues to study aging-associated post-translational modifications. *J. Vis. Exp.* **2017**, 1–8 (2017).
62. Fourest-Lieuvin, A. Purification of tubulin from limited volumes of cultured cells. *Protein Expr. Purif.* **45**, 183–190 (2006).
63. Liu, K. *et al.* GeneFishing to reconstruct context specific portraits of biological processes. *Proc. Natl. Acad. Sci. U. S. A.* **116**, 18943–18950 (2019).
64. Povea-cabello, S. *et al.* Dynamic Reorganization of the Cytoskeleton during Apoptosis: The Two Coffins Hypothesis. *Int. J. Mol. Sci.* **18**, 2393 (2017).
65. Hayot, C. *et al.* Characterization of the activities of actin-affecting drugs on tumor cell migration. *Toxicol. Appl. Pharmacol.* **211**, 30–40 (2006).
66. Lai, W. F. & Wong, W. T. Roles of the actin cytoskeleton in aging and age-associated diseases. *Ageing Res. Rev.* **58**, 101021 (2020).
67. Baird, N. A. *et al.* HSF-1-mediated cytoskeletal integrity determines thermotolerance and life span. *Science* **346**, 360–3 (2014).
68. Higuchi-Sanabria, R. *et al.* Spatial regulation of the actin cytoskeleton by HSF-1 during aging. *Mol. Biol. Cell* **29**, 2522–2527 (2018).
69. Gavrilova, L. P., Korpacheva, I. I., Semushina, S. G. & Yashin, V. A. Heat shock induces simultaneous rearrangements of all known cytoskeletal filaments in normal interphase fibroblasts. *Cell Tiss. Biol.* **7**, 54–63 (2013).
70. Duncombe, T. A. *et al.* Hydrogel Pore-Size Modulation for Enhanced Single-Cell Western Blotting. *Adv. Mater.* **28**, 327–334 (2016).
71. Drew, K. *et al.* Integration of over 9,000 mass spectrometry experiments builds a global map of human protein complexes. *Mol. Syst. Biol.* **13**, 1–21 (2017).
72. Brocchieri, L. & Karlin, S. Protein length in eukaryotic and prokaryotic proteomes. *Nucleic Acids Res.* **33**, 3390–3400 (2005).
73. Zhang, Y., Naguro, I. & Herr, A. E. In Situ Single-Cell Western Blot on Adherent Cell Culture. *Angew. Chemie - Int. Ed.* (2019).
74. Hughes, A.J., Spelke, D.M., Xu, Z., Kang, C.-C., Schaffer, D.V., Herr, A. E. Single-cell western blotting. *Nat. Methods* (2014).
75. Lee, J. P., Kassianidou, E., MacDonald, J. I., Francis, M. B. & Kumar, S. N-terminal specific conjugation of extracellular matrix proteins to 2-pyridinecarboxaldehyde functionalized polyacrylamide hydrogels. *Biomaterials* **102**, 268–276 (2016).
76. Yamauchi, K. & Herr, A. Sub-cellular western blotting of single cells. *Microsystems Nanoeng.* **3**, 16079 (2017).
77. Kang, C.-C. *et al.* Single cell-resolution western blotting. *Nat. Protoc.* **11**, 1508–1530 (2016).
78. Scrucca, L., Fop, M., Murphy, T. B. & Raftery, A. E. Mclust 5: Clustering, classification and density estimation using Gaussian finite mixture models. *R J.* **8**, 289–317 (2016).